AERODYNAMIC INTERACTIONS OF SYNCHRONIZED PROPELLERS

Nathan Welker
Department of Mechanical Engineering
Brigham Young University
Provo, Utah 84602
Email: nathandwelker@gmail.com

Daniel Maynes
Department of Mechanical Engineering
Brigham Young University
Provo, Utah 84602
Email: maynes@byu.edu

ABSTRACT

Emerging advances in electric-propulsion technology are enabling aircraft to use distributed electric propulsion (DEP) to increase efficiency and maneuverability. Distributed electric propulsion can also provide unique take-off and landing abilities which are not commonly found on traditional aircraft. The implementation of DEP effectively decreases the spacing between propellers, introducing complex aerodynamic interactions that are not well understood. This study aims to obtain experimental measurements of the flow fields of synchronized propellers at close-proximity in a side-by-side configuration using both 2D particle image velocimetry (PIV) and 3D stereoscopic PIV (SPIV) in a wind tunnel. The results of this work will be focused on identifying the impact closely-spaced propellers has on induced upwash and the formation of shed-tip vortices and how these are altered by side-to-side spacing distance and phase offset. The data can also be used for computational model validation.

1 Introduction

Recent developments in electric motors, control systems, and battery technologies are creating new opportunities to use DEP on aerial vehicles for urban air mobility. Distributed electric propulsion technology uses many small electric motors as the propulsion system for an aerial vehicle. This concept is desirable from an engineering perspective due to the scale-free nature of electric motors; unlike jet engines, scaling an electric motor up or down in size results in almost no difference in power-to-weight ratio or efficiency [1]. The concept of using DEP on aerial vehicles has many potential advantages, including increased efficiency. For example, McSwain *et al* [2] reports that NASA's Greased Lightning (GL-10) concept has demonstrated an increase in aerodynamic performance of 75% from a traditional helicopter design ($L/D_{max} = 4$). Figure 1 shows a prototype of the GL-10 in hover mode. Other advantages of DEP include increased lift, better distribution of structural loading, noise reductions, and improved maneuverability [1, 3–5].

DEP also unlocks the unique ability for aerial vehicles to perform electric vertical take-off and landing (eVTOL). Many small unmanned aerial system (UAS) vehicles, such as multirotor drones, have used eVTOL for many years. Recently, however, advances in DEP technology has sparked a potentially large future eVTOL vehicle market in urban air transportation. The Vertical Flight Society reports that there are currently over two hundred unique eVTOL aircraft concepts in development around the world [6], and Morgan Stanley Research predicts the market to increase to a $1.5

FIGURE 1: The NASA Greased Lightning (GL-10) prototype in hover mode. Credits: NASA Langley, Dave Bowman.

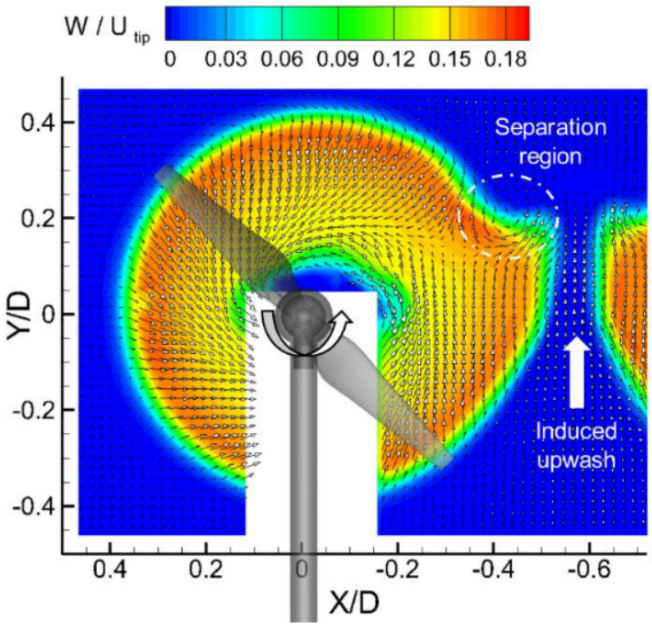

FIGURE 2: Ensemble-average velocity for the double-rotor (L=0.05D) case obtained by *et al [12].*

trillion industry by the year 2040 [7].

While DEP promises advantages and unique abilities when compared to traditional propulsion systems, it would inevitably decrease the spacing between propellers. The aerodynamic interactions of closely-spaced propellers is not well understood as it is not commonly found on conventional aircraft. Many authors have cited the importance of these rotor-to-rotor interactions [8–12] with some reporting large noise signatures and detrimental interference with decreasing rotor spacing. In one study, Alvarez *et al.* [11] modeled the interactions of rotors in a side-by-side configuration using a viscous vortex particle method. They determined that propulsive efficiency decreases across all advance ratios and Reynolds numbers as distances between rotors becomes small. They also reported large thrust fluctuations and the potentially highest noise signatures in hover and near-hover configurations.

Another study was performed by Zhou *et al* [12] who used SPIV and dynamic load measurements to determine the effects of rotor-to-rotor interactions on the aerodynamic performance of small UAVs. They concluded that thrust fluctuations would increase dramatically as the separation distance decreased, with fluctuations as high as $\sim$250% for the smallest separation ($L = 0.05D$), twin-rotor case when compared to the single-rotor case. A decrease in rotor spacing from $L = 1.0D$ to $L = 0.05D$ also resulted in a higher noise distribution. Figure 2 shows the SPIV measurement results of ensemble-averaged mean velocity contours for the twin-rotor cases. As can be seen, the flow is neither circular nor symmetric, and a region of flow separation and induced upwash can quantitatively be seen in the upper-right corner of Figure 2. The separation and upwash are likely due to the rotor-to-rotor interactions, and are hypothesized to be the cause for the strong thrust fluctuations and high noise distributions experienced in the dual rotor cases at small separation distances.

Particle image velocimetry, such as the system used by Zhou *et al*, is a standard tool used to obtain velocity and vorticity measurements of flow fields. For these systems, it is common for a high-speed camera to take multiple images of particle-induced flow illuminated by a laser at high acquisition rates [13]. For analysis of rotor flows, these images are often ob-

tained in two ways:

1. The system is triggered externally by the propeller to capture phase-locked images at a specific propeller phase angle. This provides instantaneous data that can be ensemble-averaged.
2. The images are captured with the propellers free-running to obtain data that can be time-averaged.

When studying dual-rotor interactions, both cases of data acquisition are used frequently. Historically, however, in the phase-locked case with dual-rotors, only one propeller is triggering the image acquisition while the other propeller is free-running. While data obtained from this process can provide valuable information on the flow characteristics, most computational models of multirotor flows synchronize the rotation rate of the rotors [9,11,14]. This yields the comparison between the computational studies and the experimental data much less useful. Mechanically-locking the propellers similar to the fashion used in computational models can provide data that is more valuable for model verification.

Synchronizing the propellers may also provide better insights for understanding the detrimental interference between the propellers. In one study done by Shukla *et al*. [15], the aerodynamic interactions between rotors was explored using SPIV measurements. They reported large wake interactions at smaller rotor distances resulting in a decrease in performance. They hypothesized the cause to be due to induced vortex-vortex interactions between the two propellers. In order to verify whether the adjacent rotor tip vortices is a factor in rotor performance, Shukla suggests mechanically linking the rotors together to synchronize their rotation rates.

This study aims to obtain both 2D and 3D flow field measurements of the interactions of two propellers in a wind tunnel. An experimental apparatus housing two mechanically-linked propellers was built. A triggering device was constructed to obtain images at specific propeller phase angles. A high-resolution PIV system allows acquisition of ensemble-averaged velocity and vorticity fields processed from the phase-locked PIV images. Various propeller spacings and propeller phase offsets are to be explored. The results of the tests are focused on identifying the interactions between closely-spaced propellers and what impact they have on induced upwash and the formation of shed-tip vortices and how these impacts vary with separation distance and propeller phase offset. The data can also be used for computational model validation.

2 Methods

2.1 Facility

The experimental investigations are performed in the BYU Engineering Research Lab using the large Aerolab wind tunnel. The tunnel has a 120 mph maximum speed, a 4 ft $\times$ 3 ft $\times$ 14 ft test section, and a contraction ratio of 5:1.

2.2 Experimental Apparatus

The experimental apparatus consists of two propeller stands housed by aerodynamic shrouds. The aerodynamic shrouds are designed to provide minimal obstruction downstream of the propellers for more accurate PIV results. They have been constructed by 3D printing ABS plastic. The two shrouds are identical in shape and size but have differing internal components. One of the stands consists of a single motor which provides rotation to two DJI 9443 propellers. This shroud also contains an optical rotation sensor used to generate a cyclic signal. An external triggering device converts the cyclic signal to a TTL signal which is then be used to trigger the PIV system at specific propeller phase angles. A shaft and miter gear system mechanically links the rotation of the two propellers together. Mechanically-linking the rotation is advantageous as it provides data more useful to computational model validation. The motor side of the experimental apparatus is shown in Figure 3.

2.3 PIV System and Processing

Figure 4 shows the 2D PIV setup of this study. It consists of a high-resolution PIV system, the external triggering device, and the experimental apparatus.

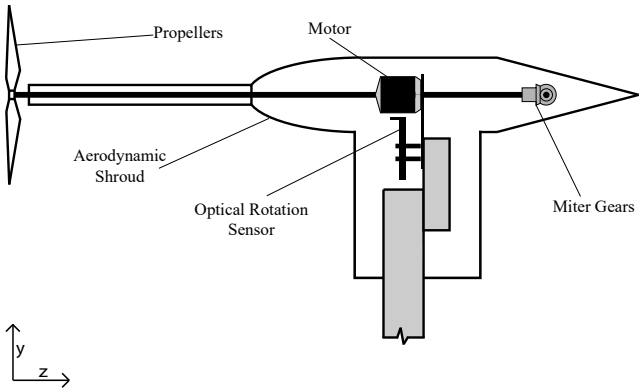

FIGURE 3: The motor side of the experimental apparatus designed for obtaining flow field measurements.

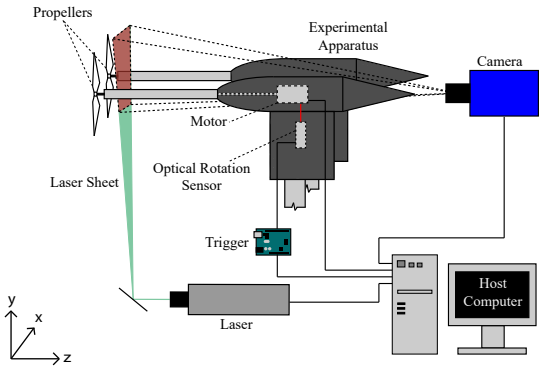

FIGURE 4: General setup for PIV measurement acquisition.

The PIV system is used to obtain flow-field measurements of the two propellers. A LaVision droplet generator introduces oil particles approximately 1 µm in diameter to the air flow. A double-pulsed Nd:YAG laser emitting two 200 mJ pulses with a 532 nm wavelength is used to illuminate the particles. A high-resolution LaVision Imager Intense camera is used to obtain the PIV image pairs of the illuminated particles. The time delays between the two images are between 50 to 200 µs.

Figure 5 shows the 3D SPIV setup of this study. It consists of the same components as the 2D PIV setup,

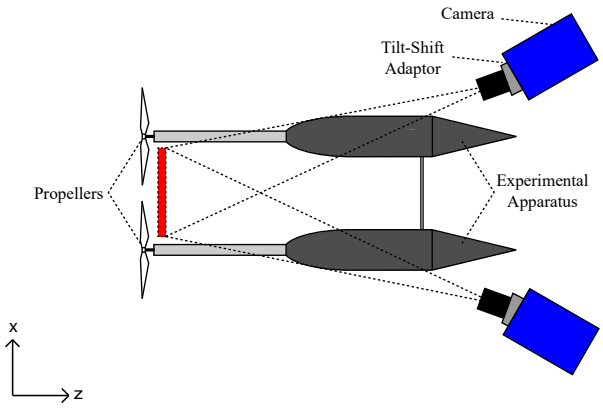

FIGURE 5: Setup for SPIV measurement acquisition.

but has an added high-resolution LaVision Imager Intense camera and two tilt-shift adaptors to account for the Scheimpflug principle [16].

One plane of view is explored during experimentation. It is a set of planes in the spanwise XY plane (using the XYZ axis convention of fig 4) at various Z distances between $0.05D$ to $1.0D$ downstream from the propellers (where D is the propeller diameter). An example of this plane is shown in Figures 4 and 5.

Another plane of interest would be in the streamwise XZ plane intersecting the propeller axes and directly downstream of the propellers. Details of the specific tests are as follows:

- 500 ensemble-averaged SPIV images at each phase angle (θ) between 0° to 180° in 30° increments in the spanwise XY plane shown in Figure 5:

1. Hover condition with a single rotational speed
   (a) Single propeller "control" case
2. Hover condition with a single rotational speed at five propeller spacings ($L = 0.05D$, $0.1D$, $0.25D$, $0.5D$, $1.0D$) for each case:
   (a) Phase-locked with dual, counter-rotating propellers
   (b) Phase-offset with dual, counter-rotating propellers

- 500 ensemble-averaged SPIV images at each phase angle between 0° to 180° in 30° increments. The plane of focus is in the streamwise XZ plane intersecting the propeller axes in the propeller interaction region. The same separation distances and propeller cases as above will be explored.

Rotational speed was determined based on values used by other researchers conducting computational simulations.

The instantaneous flow velocity vector fields are obtained by post-processing the images. This is done by performing 2 passes of a cross-correlation technique with an interrogation window size of 48 $\times$ 48 pixels and an effective overlap of 50% followed by two passes with an interrogation window of size 24 $\times$ 24 and an effective overlap of 50%. Average flow velocity vector fields are obtained from ensemble-averaging the post-processed images. The velocity and vorticity flow fields can be used to answer the fundamental questions of the behavior of the flow physics. The data can also be compared to computational models for validating the specific scenarios and cases outlined above.

3 Results and Discussion

3.1 Progress to Date

3.1.1 Phase-Locked Tests The first test conducted was a single propeller case to be used as a control to compare to the dual propeller cases. Figure 6 shows the field of view and angle notation for the experiments. The SPIV images were taken phase-locked at six different θ positions at a plane $0.05D$ downstream from the propeller. The images were post-processed and ensemble-averaged to obtain average flow velocity vector fields. This vector field phase-locked at $\theta = 150°$ is shown in Figure 7. The colors signify flow in the Z-direction (into the page) while the arrows signify flow in the XY plane.

The next tests were performed with the following dual, counter-rotating, synchronized cases: in-phase and 90° out of phase (Figure 8 illustrates the difference between the two cases). The propellers were separated at a distance of $L/D = 0.1$ and at the same x-position as the single propeller case. Figures 9 and 10 show the vector field phase-locked at $\theta = 150°$ for the in-phase and 90° out of phase cases, respectively.

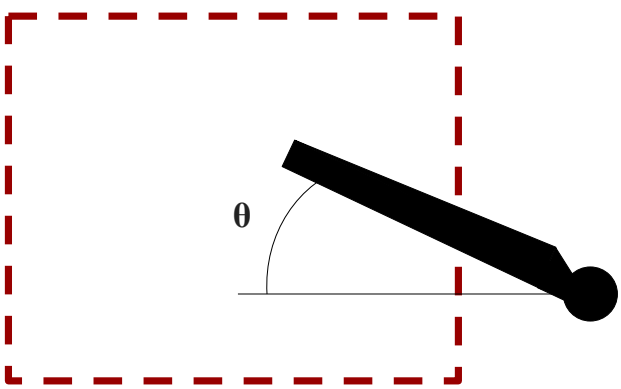

FIGURE 6: The field of view and angle notation for the initial experiments (the phase angle is measured from the leading edge of the propeller).

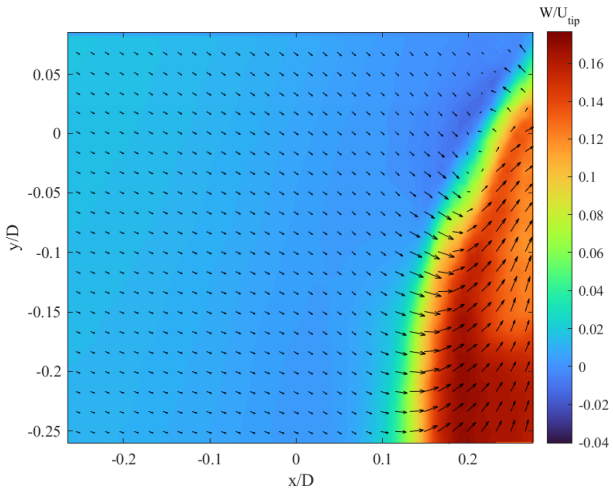

FIGURE 7: Ensemble-averaged velocity vector field of the spanwise phase-locked flow at $\theta = 150°$ for the single propeller case.

Both dual cases appear to have a larger zone of interaction than the single propeller case, as is evident by the larger area of Z-direction velocity between the two propellers. However, the interacting propellers

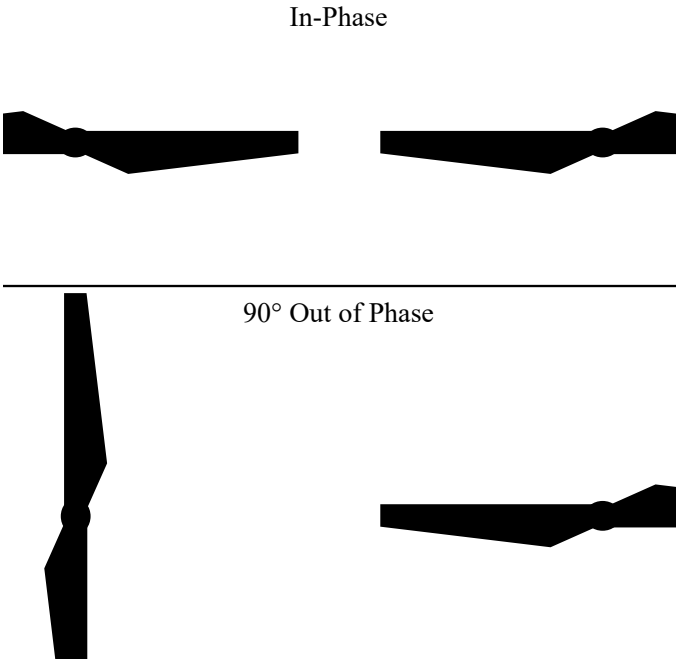

FIGURE 8: Phase notation for the dual propeller cases.

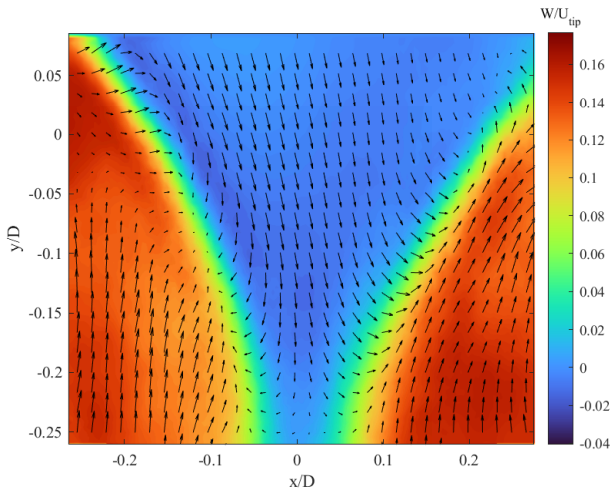

FIGURE 9: Ensemble-averaged velocity vector field of the spanwise phase-locked flow at $\theta = 150°$ for the dual, in-phase propeller case.

appear to have little effect on the other features of the propeller wakes. For example, the propeller tip vortex can clearly be seen to be at the same position around $x/D = 0.2$ and $y/D = -0.025$ for both the single and

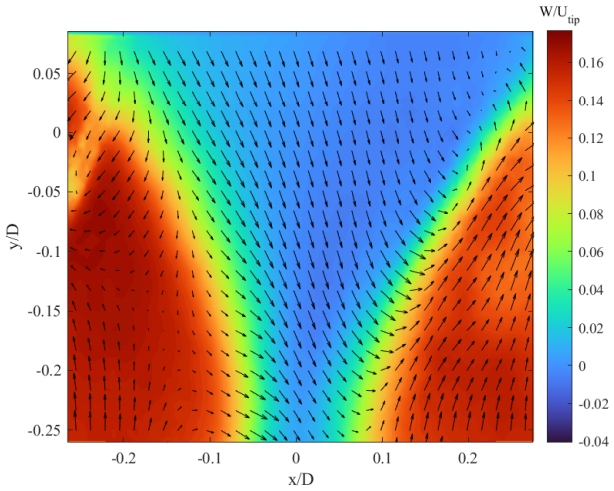

FIGURE 10: Ensemble-averaged velocity vector field of the spanwise phase-locked flow at $\theta = 150°$ for the dual, 90° out of phase propeller case. The phase angle was measured from the propeller represented by the right side of the vector field.

the two dual cases.

It can be seen that while they appear similar, there are subtle differences between the two dual cases. The right propeller for both cases appear similar in magnitude and shape. The left propeller, however, appears to differ for the out of phase case. This is expected, as the right propeller for both cases were locked to the same phase angle, while the left was 90° off in the out of phase case.

3.1.2 Phase-Averaged Test The next test involved obtaining a larger field of view of the propellers to compare against the results obtained by Zhou *et al* as shown in Figure 2. The test involved acquiring 500 images of the synchronized, in-phase propellers. The propellers were set to "free run" (ie. the triggering mechanism was not used). This resulted in an average velocity field over all phase angles, which is shown in Figure 11.

Comparing the results from the phase-averaged test to the test conducted by Zhou *et al* shows that the general shape and magnitude of the Z-component

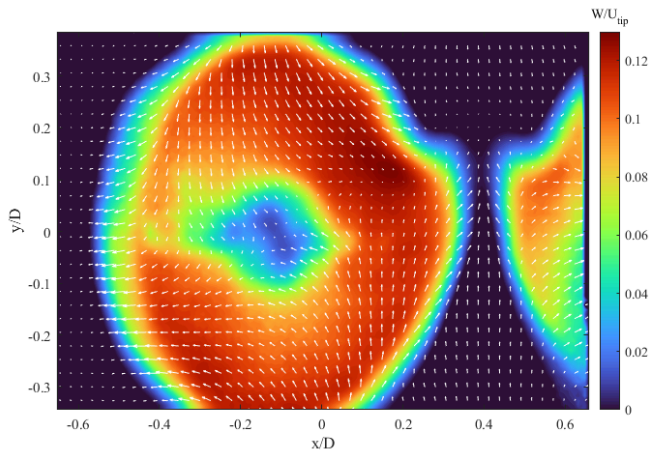

FIGURE 11: Ensemble averaged SPIV results for synchronized, free-running propellers at a separation distance of $L/D = 0.05$.

of velocity is relatively similar. The separation region and induced upwash in the XY plane is seen around the same locations as well. Differences arise, however, when looking at the behavior of XY flow velocity on the left side propellers. The results from Zhou *et al* shows a uniform velocity directed around the center of the propeller in the rotation of direction. The results from this present study shows a velocity direction being deflected outward from the propeller. This is possibly due to sub-optimal particle seeding in this area during the experiment, but further testing is needed to prove this hypothesis.

3.2 Future Work

The next step is to perform SPIV measurements to obtain flow velocity vector fields at the other propeller spacings mentioned previously with the propellers in the single, dual in-phase, and dual out of phase orientations. These will be taken phase-locked at 30° increments with the larger field of view shown in Figure 11. These will be analyzed to determine the differences between the various cases and their effect on the propeller wake interactions and other flow features.

Other test will also be conducted in the streamwise XZ plane to view the effect of propeller spacing, phase angle, and propeller synchronization on the formation of shed-tip vortices.

4 Conclusion

An experimental apparatus capable of providing mechanically-linked rotation to two propellers was manufactured. A high-resolution system was used to obtain SPIV images of the interaction region between two propellers. In one set of tests, a single propeller control case was compared to two dual propeller cases: in-phase and 90° out of phase. A larger zone of Z-direction velocity was seen in both of the dual cases when compared to the single case. Another test was performed involving a larger field of view to compare to the results from Zhou *et al*. The results were similar in Z-direction velocity, but showed differences in XY velocity shape. This is hypothesized to be due to poor particle seeding during experimentation. The next step is to perform the same SPIV measurements for the single and dual cases at other separation distances. Future work will also include obtaining more velocity fields at other separation distances, propeller phase offsets, and at other planes of interest. The results of these tests will help determine the effect separation distance and phase offset have on the induced upwash and tip vortex formation of the propellers. The experimental measurements of the flow field obtained from this study will also be provided to another researcher and will serve as a source of model validation for computational models.

REFERENCES

[1] Moore, M. D., and Fredericks, B., 2014. "Misconceptions of electric propulsion aircraft and their emergent aviation markets". *52nd Aerospace Sciences Meeting*, pp. 1–17.

[2] Mcswain, R. G., Glaab, L. J., and Theodore, C. R., 2017. "Greased Lightning (GL-10) Performance Flight Research – Flight Data Report NASA STI Program . . . in Profile".

[3] Ko, Y.-Y. A., 2003. "The Multidisciplinary Design Optimization of a Distributed Propulsion Blended-Wing-Body Aircraft". pp. 1–222.

[4] Gohardani, A. S., 2013. "A synergistic glance at the prospects of distributed propulsion technology and the electric aircraft concept for future unmanned air vehicles and commercial/military aviation". *Progress in Aerospace Sciences,* ***57***, pp. 25–70.

[5] Stoll, A. M., Bevirt, J. B., Moore, M. D., Fredericks, W. J., and Borer, N. K., 2014. "Drag Reduction Through Distributed Electric Propulsion". *AIAA AVIATION 2014 -14th AIAA Aviation Technology, Integration, and Operations Conference*(June), pp. 16–20.

[6] Sherman, J., 2019. Vertical Flight Society Reports More than 200 eVTOL Aircraft Now in Development Electric Vertical Takeoff and Landing Aircraft Projects Double in Past Year, sep.

[7] Rep., T., 2018. Flying Cars: Investment Implications of Autonomous Urban Air Mobility. Tech. rep., Morgan Stanley Research.

[8] Ning, Z., 2018. "Experimental investigations on the aerodynamic and aeroacoustic characteristics of small UAS propellers". PhD thesis, Iowa State University.

[9] Yoon, S., Lee, H. C., and Pulliam, T. H., 2016. "Computational Analysis of Multi-Rotor Flows". *54th AIAA Aerospace Sciences Meeting*(January), pp. 1–11.

[10] Theys, B., Dimitriadis, G., Hendrick, P., and De Schutter, J., 2016. "Influence of propeller configuration on propulsion system efficiency of multi-rotor Unmanned Aerial Vehicles". In 2016 International Conference on Unmanned Aircraft Systems, ICUAS 2016.

[11] Alvarez, E. J., and Ning, A., 2019. "Modeling Multirotor Aerodynamic Interactions Through the Vortex Particle Method". *AIAA Aviation Forum*.

[12] Zhou, W., Ning, Z., Li, H., and Hu, H., 2017. "An Experimental Investigation on Rotor-to-Rotor Interactions of Small UAV". *35th AIAA Applied Aerodynamics Conference, 2017*(June), pp. 1–16.

[13] Westerweel, J., Elsinga, G. E., and Adrian, R. J., 2013. "Particle Image Velocimetry for Complex and Turbulent Flows". *Annual Review of Fluid Mechanics,* ***45***(1), pp. 409–436.

[14] Aref, P., Ghoreyshi, M., Jirasek, A., Satchell, M. J., and Bergeron, K., 2018. "Computational study of propeller-wing aerodynamic interaction". *Aerospace,* ***5***(3), pp. 1–20.

[15] Shukla, D., and Komerath, N., 2018. "Multirotor Drone Aerodynamic Interaction Investigation". *Drones,* ***2***(4), p. 43.

[16] Scheimpflug, T., UK Patent GB190401196A, Jan. 1904. Improved method and apparatus for the systematic alteration or distortion of plane pictures and images by means of lenses and mirrors for photograpy and for other purposes.